Journal of Alloys and Compounds 817 (2020) 152761

Contents lists available at ScienceDirect

Journal of Alloys and Compounds

journal homepage: http://www.elsevier.com/locate/jalcom

The effect of Sm^{3+} co-doping on the luminescence properties of $Ca_{2\cdot85}Li_{0\cdot15}(PO_4)_{1\cdot85}(SO_4)_{0.15}$: Dy^{3+} white-emitting phosphors

Meng Yu [a, b], Xinru Xu [a], Wentao Zhang [a, *], Xianfei Chen [a], Peicong Zhang [a], Yi Huang [c, **]

[a] College of Materials and Chemistry & Chemical Engineering, Chengdu University of Technology, Chengdu, 610059, China
[b] College of Energy, Xiamen University, Xiamen, 361102, China
[c] State Key Laboratory of Geohazard Prevention and Geoenvironment Protection, College of Ecology and Environment, Chengdu University of Technology, Chengdu, 610059, China

ARTICLE INFO

Article history:
Received 10 August 2019
Received in revised form
20 October 2019
Accepted 21 October 2019
Available online 23 October 2019

Keywords:
$Ca_3(PO_4)_2$
Phosphor
Partial substitution
Luminescence enhancement
Warm white emission

ABSTRACT

A novel white emitting phosphate-based phosphor $Ca_{3-x}Li_x(PO_4)_{2-x}(SO_4)_x$:$Dy^{3+}$, Sm^{3+} with high emission intensity and lower correlated color temperature were successfully synthesized via the sol-gel method.

The structures of these prepared phosphors matched well with standard $Ca_3(PO_4)_2$. The Dy^{3+}-doped $Ca_{3-x}Li_x(PO_4)_{2-x}(SO_4)_x$ phosphors showed white luminescence via the combination of blue (487 nm) and yellow (578 nm) emissions, which were attributed to the $^4F_{9/2} \rightarrow {}^6H_{15/2}$ and $^4F_{9/2} \rightarrow {}^6H_{13/2}$ electron transitions of Dy^{3+}, respectively. The synthesized phosphor exhibited a significant enhancement in luminescence intensity at the optimum value of $x = 0.15$. With the incorporation of Sm^{3+}, a warm white emission with lower correlated color temperature (4281 K) was achieved in Dy^{3+}/Sm^{3+} co-doped samples. The obtained external quantum efficiency reached 21.7% in the optimized phosphor. The improved performance was strongly associated with red emission supplemented by Sm^{3+}, and it demonstrated the existence of efficient energy transfer between the Dy^{3+} and Sm^{3+} ions ($^4F_{9/2} \rightarrow {}^4G_{7/2}$ and $^4F_{9/2} \rightarrow {}^4G_{5/2}$). Overall, the investigation carried out by us has revealed that the luminescence properties of $Ca_3(PO_4)_2$ phosphor can be significantly improved through Li^+/S^{6+} partial substitution and Dy^{3+}/Sm^{3+} co-doping.

1. Introduction

Regarded as a representative of next-generation solid-state lighting technologies, white light-emitting diodes (*w*-LEDs) possess outstanding characteristics in comparison with traditional lighting sources. The most prominent advantages are their higher luminous efficiency, lower environmental impact, longer lifetime and flexible application [1–4]. In the past few decades, considerable effort has been devoted to the exploration of their properties and applications. Currently, the most common method for fabricating *w*-LEDs is combining a blue-emitting chip (GaN/InGaN) with a yellow-emitting phosphor (YAG: Ce^{3+}) [5,6], and it has been widely used for commercial manufacture of phosphors. However, the white light generated by this approach encounters a poor color rendering index (*CRI* < *80*) and high correlated color temperature (*CCT*) for the absence of a red light component [7–9].

In order to address this deficiency with YAG: Ce^{3+} phosphor, researchers have come up with another alternative to achieve *w*-LEDs via near-ultraviolet (n-UV) excitation for tricolor (red, blue and green) phosphors [10–12]. Unfortunately, there is an inevitable interference between different phosphor components, giving rise to uncoordinated emission, poor light absorption, low luminous efficiency, as well as a higher fabrication cost. These drawbacks pose challenges to the development and large-scale application of phosphor-based LED lighting technologies. Therefore, the demand for developing novel phosphor with higher luminescence intensity and better lighting quality stimulates extensive research.

Until now, diverse methods have been attempted to ameliorate the properties of phosphors, such as synthesis method optimization [13,14], cationic/anionic substitution [15–17], rare-earth (RE) ions codoping as well as simulation optimization [18], *etc.* It is noteworthy that cationic/anionic substitution has been widely studied in recent years [15–17,19]. Specifically, Wang. et al. [15] investigated the influence of substitution of Si by Al^{3+}/P^{5+} ions substitution on the structure and luminescence properties of Sr_2SiO_4:Eu^{2+} phosphors. Both the luminescence intensity and

* Corresponding author.
** Corresponding author.
E-mail addresses: zhangwentao2005@163.com (W. Zhang), huangyi@cdut.cn (Y. Huang).

https://doi.org/10.1016/j.jallcom.2019.152761
0925-8388/

lifetime were enhanced with Al^{3+}/P^{5+} substitution, which can be attributed to the change of crystal field around Eu^{2+}, as a result, Eu^{2+} presented the preference to occupy Sr(I) and Sr(II) sites in the host lattice. Moreover, S. A. Khan et al. [16] have recently reported the improved photoluminescence properties and thermal stability in $Ba_2Si_5N_8:Eu^{2+}$ phosphor through partial substitution of Al−O for Si−N. A detailed explanation from the view of lattice expansion was given. The substitution of large Al−O for Si−N leads to the expansion of the host lattice, which decreases the concentration of traps, meanwhile, and the variation in the structural environment of Eu^{2+} activators favors its efficient occupation by in $Ba_2Si_{(5-x)}Al_xN_{(8-x)}O_x$ phosphors host lattice. These studies reveal that cationic/anionic substitution can be adopted as an effective approach for optimization in the properties of phosphor.

Generally, RE ions play a critical role in phosphor-based LED technologies thanks to their diverse energy transition. For example, trivalent dysprosium ion (Dy^{3+}) possesses a series of characteristic transition of $^4F_{9/2} \rightarrow {}^6H_{I/2}$ (I = 9, 11, 13, 15). Especially, the dominant emission peaks of Dy^{3+} located in blue (~480 nm) and yellow (~580 nm), corresponding to the magnetic dipole transition ($^4F_{9/2} \rightarrow {}^6H_{15/2}$) and the electric dipole transition ($^4F_{9/2} \rightarrow {}^6H_{13/2}$), respectively. Hence, the combination of blue and yellow enable it to emit white emission [20–22].

Additionally, recent studies have also suggested that the luminescence of Dy^{3+} is strongly affected by the crystal structure [23,24]. For instance, in Yu et al.' s experimental work [23], the emission intensity of Dy^{3+} in $Ca_{1-x}Gd_xF_{2-x}$ single crystal was dramatically improved compared with that of Gd^{3+} free samples. The Gd^{3+} not only serves as buffer ions to regulate the local lattice structure of Dy^{3+} ions, but also facilitates the energy transfer from Gd^{3+} to Dy^{3+}, and a tunable white-light emission was achieved through the optimization in Gd^{3+} concentration.

Nevertheless, as we mentioned above, Dy^{3+} single-doped samples would also suffer from defects like low *CRI* and high *CCT* value due to insufficient red emission. Similar to cationic/anionic substitution, ions-codoping has attracted tremendous interest with attention being given to its extraordinary role in tunable emission [25–27]. One can notice that Sm^{3+} has been widely used as an appropriate activator ion in red-emitting phosphor due to its $^4G_{5/2} \rightarrow {}^6H_{I/2}$ (I = 5, 7, 9) transitions, result in a series of strong emission peaks ranging from orange to red [28,29]. Accordingly, it indicates that novel Dy^{3+} and Sm^{3+} co-doping could be a potential solution to lack of red emission, as a consequence, a warm white emission can be achieved.

Over the past few decades, continuous attention has been paid to the development of host materials, including phosphate, nitrides, sulfides, aluminates, and silicates, *etc* [8,10,14,17,30]. In particular, phosphate has attracted widespread attention for their better performance like superior efficiency and excellent stability and lower cost among the various candidates [31–33]. Considerable research has been carried out on phosphate-based luminescent materials that follow the general expression $M_3(PO_4)_2$ (M = Ca, Sr, Ba) and $M_5(PO_4)_3X$ (M = Ca, Sr, Ba, X = F, Cl, Br), such as $Ca_3(PO_4)_2:Eu^{3+}$ [34], $Ca_3Sr_3(PO_4)_4:Sm^{3+}$ [35], $(Ca_{1-x}Ba_x)_3(PO_4)_2:Eu^{2+}$ [36], $Sr_5(PO_4)_3F$ [37,38]. These studies indicate that $Ca_3(PO_4)_2$ can be adopted as a suitable host single-component phosphor.

In this paper, a series of $Ca_{3-x}Li_x(PO_4)_{2-x}(SO_4)_x:Dy^{3+}/Sm^{3+}$ phosphors were synthesized by the sol-gel method. The introduction of Li^+ and S^{6+} ions was expected to substitute the Ca^{2+} and P^{6+}, result in a lattice distortion, so as to change the surrounding environment of Dy^{3+} activators. On the one hand, Li^+ and S^{6+} (r_{Li^+} = 0.076 nm, $r_{S^{6+}}$ = 0.037 nm) have close radii to Ca^{2+} and P^{5+} ($r_{Ca^{2+}}$ = 0.099 nm, $r_{P^{5+}}$ = 0.038 nm). Given that the replacement of large Ca^{2+}/P^{5+} by small Li^+/S^{6+}, it will cause a lattice contraction to the surrounding of activators. On the other hand, this incorporation of Li^+/S^{6+} will not affect the charge balance of the host. Therefore, this cationic/anionic substitution was carried out on $Ca_3(PO_4)_2:Dy^{3+}$ phosphor. Subsequently, upon the determination of the optimized substitution ratio of Li^+/S^{6+}, Sm^{3+} was co-doped in $Ca_{3-x}Li_x(PO_4)_{2-x}(SO_4)_x:Dy^{3+}$ phosphor to supplement the red light emission. In consequence, a warm white emission with low CCT value was obtained. Systematic investigation of the effects of partial substitution of Ca^{2+} and P^{5+} with Li^+ and S^{6+} ions, and Dy^{3+}/Sm^{3+} doping concentration on the structures and luminescence properties of $Ca_{3-x}Li_x(PO_4)_{2-x}(SO_4)_x:Dy^{3+}$, Sm^{3+} samples was performed. This study presents a deep insight into the effect of cationic/anionic substitution and RE ions co-doping on the properties amelioration in phosphate phosphor, and the results suggest this type of phosphor has great potential for application in *w*-LEDs.

2. Experimental

All $Ca_{3-x}Li_x(PO_4)_{2-x}(SO_4)_x:yDy^{3+}, zSm^{3+}$ samples were prepared using a simple sol-gel method. The synthesis amount of $Ca_3(PO_4)_2$ is determined as 0.01 mol. The substitution amount of Ca^{2+}/P^{5+} ranged from stoichiometric values of 0–0.25. The doping concentration of Dy^{3+} and Sm^{3+} ions was controlled as 1 mol% ≤ y ≤ 5 mol % and 0.5 mol% ≤ z ≤ 3 mol%, respectively. For $Ca_{2.85}Li_{0.15}(PO_4)_{1.85}(SO_4)_{0.15}$:3%$Dy^{3+}$, 3%$Sm^{3+}$ sample, 0.0285 mol $Ca(NO_3)_2 \cdot 4H_2O$ (6.7302 g), 0.0185 mol $NH_4H_2PO_4$ (2.1278 g), 0.01425 mol $C_6H_8O_7$ (2.994 g), 0.00075 mol $Li_2SO_4 \cdot H_2O$ (0.0959 g), 0.00075 mol $(NH_4)_2SO_4$ (0.0090 g), 0.0003 mol $Dy(NO_3)_3 \cdot 6H_2O$ (0.1369 g), 0.0003 mol $Sm(NO_3)_3 \cdot 6H_2O$ (0.1338 g) were weighed as starting materials according to stoichiometric ratio. Firstly, $Ca(NO_3)_2 \cdot 4H_2O$, $C_6H_8O_7$, $Dy(NO_3)_3$ and $Sm(NO_3)_3$ were added to a beaker containing deionized water to form a stable solution. Subsequently, the appropriate quantities of $NH_4H_2PO_4$, $Li_2SO_4 \cdot H_2O$ and $(NH_4)_2SO_4$ were added to the above solution, and the solution was mixed by magnetic stirrer at 75 °C to form a transparent sol. Then, the sol was placed in an oven at 120 °C for 24 h to dry thoroughly until the color changed to transparent yellow. Finally, the dried gel was placed in a crucible and transferred to a furnace. It was heated to 1000 °C at a rate of 10 °C per minute and the temperature maintained for 2 h then cooled naturally to room temperature. The as-prepared dried gel was then ground into a powder in an agate mortar for subsequent testing and characterization.

The crystal structures of the obtained phosphors were characterized using X-ray diffraction (XRD) performed on an X-ray diffractometer (DX-2700, Aolong Company, China) with Cu Kα radiation (λ = 1.5406 Å). The morphology and elemental composition of the samples were confirmed using a scanning electron microscope (SEM, JSM-7800F, JEOL, Japan) and Energy Dispersive Spectroscopy (EDS). Photoluminescence (PL) spectra were measured by a luminescence spectrometer (F-4600, Hitachi, Japan) with a 150 W Xe lamp as the excitation source. The quantum efficiency of samples was obtained by a QEMS 2000. All phosphor characterization results were obtained at room temperature.

3. Results and discussion

Fig. 1 shows the XRD patterns for a series of $Ca_{3-x}Li_x(PO_4)_{2-x}(SO_4)_x$:2%$Dy^{3+}$ samples prepared at 1000 °C. XRD analysis revealed that $Ca_{3-x}Li_x(PO_4)_{2-x}(SO_4)_x$:2%$Dy^{3+}$ (x = 0, 0.05, 0.1, 0.15 and 0.2) samples were indexed with an orthorhombic lattice and a space group of *R3c* [39]. All the patterns were consistent with standard data for $Ca_3(PO_4)_2$ (PDF card no. 09–0169), and a weak impurity peak of $Ca_5(PO_4)_3(OH)$ (PDF card no. 09–0432) is marked in Fig. 1. In addition, no apparent impurity phases corresponding to Li^+, S^{6+} or Dy^{3+} were detected, indicating that small amounts of ion

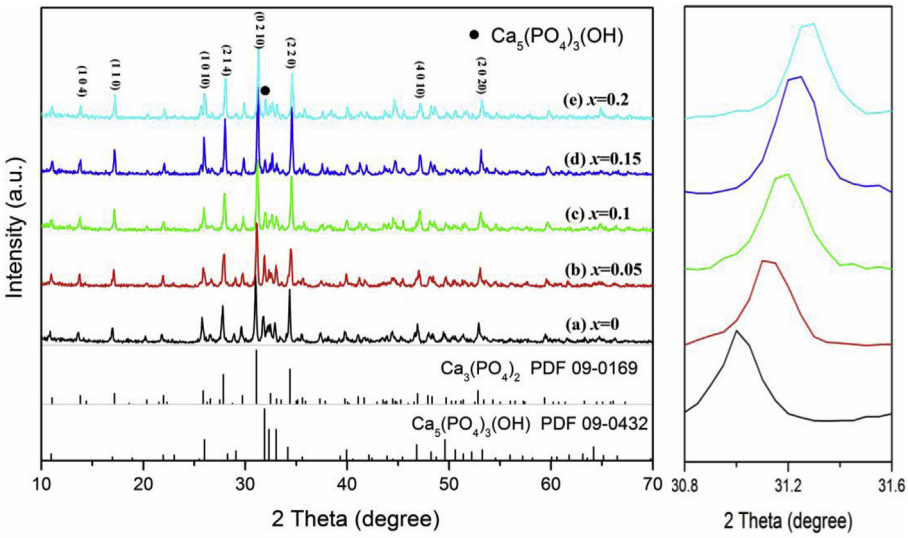

Fig. 1. XRD patterns of $Ca_{3-x}Li_x(PO_4)_{2-x}(SO_4)_x$:2%$Dy^{3+}$ phosphors with different x values and the magnification pattern of (0 2 10) crystal face.

doping did not cause significant changes in the host structure. With the increase of substitution ratio *x* from 0 to 0.2, the diffraction peak gradually shifts to a larger angle as shown in the magnificent part of $2\theta = 30.8°-31.6°$, and the cell volume of the samples slightly decreased, accompanied with a small lattice distortion (see Table 1). This can be attributed to their similar ionic radii, Ca^{2+} (0.099 nm), Dy^{3+} (0.091 nm), Li^{+} (0.076 nm), P^{5+} (0.038 nm) and S^{6+} (0.037 nm). More specifically, the substitution of small Li^{+}/S^{6+} ($r_{Li^{+}} + r_{S^{6+}} = 0.113$ nm) for large Ca^{2+}/P^{5+} ($r_{Ca^{2+}} + r_{P^{5+}} = 0.137$ nm) ions resulted in the lattice contraction around Dy^{3+} activators, causing the lattice contraction and shift of XRD peaks to larger 2 θ angles [16]. It can also be seen that the intensities of diffraction peaks become stronger after ionic substitution; this result demonstrated that Li^{+} and S^{6+} ions improved the crystallinity without affecting the charge balance [40,41].

Detailed structural parameters of these samples were obtained by the Rietveld refinement method via the GSAS program. Fig. 2 shows the Rietveld refined XRD pattern of the $Ca_{2.85}Li_{0.15}(PO_4)_{1.85}(SO_4)_{0.15}$:2%$Dy^{3+}$ phosphor. These results confirmed that this phosphor belongs to an orthorhombic R-3c space group, and its lattice parameters were determined as a = 10.429 Å, b = 10.429 Å and c = 37.38 Å. The refinement factors converged to $R_{wp} = 5.8\%$, $R_p = 4.16\%$ and $\chi^2 = 2.36$, indicating a good-quality fit.

To investigate the micromorphology and elemental composition of the as-prepared $Ca_3(PO_4)_2$:2%Dy^{3+} and $Ca_{2.85}Li_{0.15}(PO_4)_{1.85}(SO_4)_{0.15}$:2%$Dy^{3+}$ samples, SEM images and EDS results were obtained (Fig. 3). The SEM images revealed smooth, spherical particles with homogenous size distribution and grain diameters of approximately 120–160 nm. The grain diameter

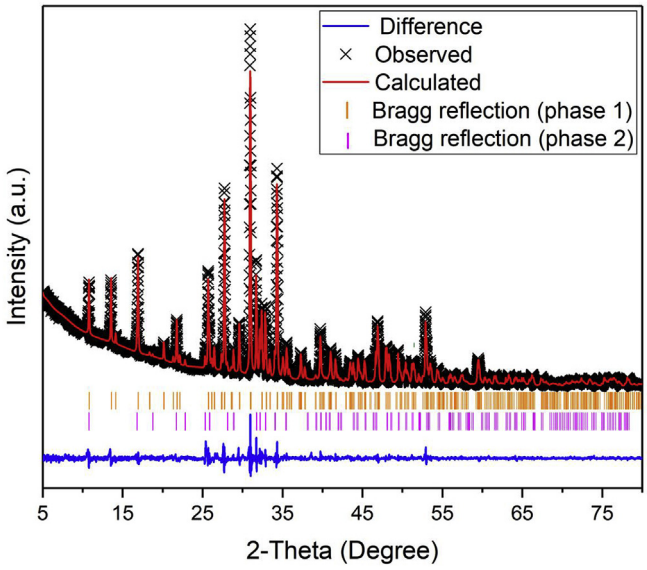

Fig. 2. The Rietveld refinement of $Ca_{2.85}Li_{0.15}(PO_4)_{1.85}(SO_4)_{0.15}$:2%$Dy^{3+}$ sample.

slightly increases with the introduction of Li^{+}, that's because Li^{+} could decrease the crystallization temperature and cause crystals agglomeration. The EDS showed that $Ca_{2.85}Li_{0.15}(PO_4)_{1.85}(SO_4)_{0.15}$:2%$Dy^{3+}$ contained Ca, P, S, Dy, and O, indicating that the doped Dy^{3+} was distributed in the lattice of $Ca_{2.85}Li_{0.15}(PO_4)_{1.85}(SO_4)_{0.15}$. (Due to its low energy, elemental Li cannot be detected by EDS.) The percentage of each element in $Ca_{2.85}Li_{0.15}(PO_4)_{1.85}(SO_4)_{0.15}$:2%$Dy^{3+}$ as verified by EDS was Ca 20.78%, P 13.52%, S 0.96%, Dy 0.31% and O 64.43%, and the stoichiometric atomic ratio of each element was Ca 22.08%, P 14.33%, S 1.16%, Dy 0.46% and O 61.97%. The composition suggested by EDS was consistent with the stoichiometric weight ratio within reasonable error. For obtaining some more precise results especially Li content, the XRF measure has been carried and the corresponding result has listed in Table 2, which shows the precise composition with the stoichiometric ratio of $Ca_{2.85}Li_{0.15}(PO_4)_{1.85}(SO_4)_{0.15}$:2%$Dy^{3+}$.

To determine the optimal substitution ratio, the emission

Table 1
The lattice parameters and volume of $Ca_{3-x}Li_x(PO_4)_{2-x}(SO_4)_x$ crystals with different *x* value.

Samples	a/Å	b/Å	c/Å	V/Å^3
$x = 0$	10.4409	10.4409	37.4396	3534.59
$x = 0.05$	10.4357	10.4357	37.4317	3530.37
$x = 0.1$	10.4371	10.4371	37.3836	3529.03
$x = 0.15$	10.4285	10.4285	37.4145	3526.77
$x = 0.2$	10.4211	10.4211	37.5522	3523.88
$x = 0.25$	10.4245	10.4245	37.4000	3519.77

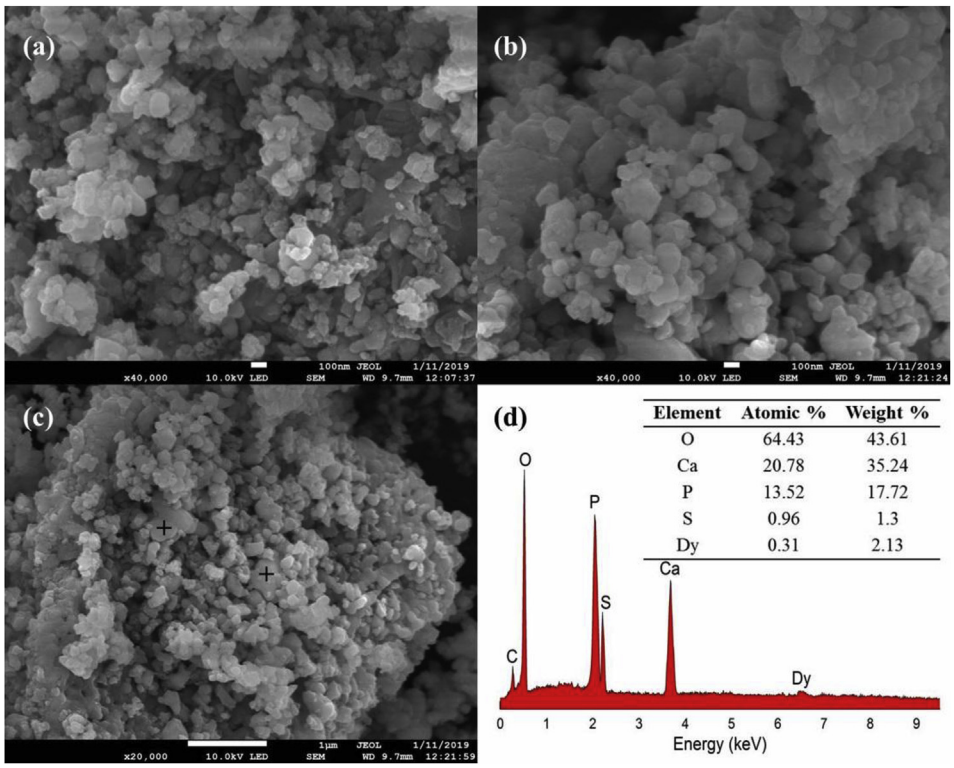

Fig. 3. SEM image and EDS element components of $Ca_3(PO_4)_2$:2%Dy^{3+} and $Ca_{2.85}Li_{0.15}(PO_4)_{1.85}(SO_4)_{0.15}$:2%$Dy^{3+}$ samples.

Table 2
XRF result of $Ca_{2.85}Li_{0.15}(PO_4)_{1.85}(SO_4)_{0.15}$:2%$Dy^{3+}$ sample.

Elements	Content (%)
CaO	50.11
P_2O_5	40.29
SO_3	3.63
Li_2O	0.65
Dy_2O_3	5.32

spectra (λ_{ex} = 352 nm) of $Ca_{3-x}Li_x(PO_4)_{2-x}(SO_4)_x$:2%$Dy^{3+}$ samples were obtained (Fig. 4). Two strong emission peaks were observed at 487 nm (blue) and 578 nm (yellow), which could be attributed to the $^4F_{9/2} \rightarrow {}^6H_{15/2}$ and $^4F_{9/2} \rightarrow {}^6H_{13/2}$ transitions of Dy^{3+} ions, respectively. This means the white emission could be achieved through the combination of blue and yellow emissions. Compared with the unsubstituted sample, the luminescence intensities of the substituted samples were significantly enhanced through the incorporation of Li^+ and S^{6+} ion pairs, the maximum intensity appears at $x = 0.15$, and then it progressively decreases. This was because the introduction of Li^+/S^{6+} ions resulted in a little lattice distortion, which changing the crystal fields around the Dy^{3+} ions and improving the emission intensity. However, too large substitution ratio caused the appearance of $Ca_5(PO_4)_3OH$ impurity and increased the possibility of non-radiation transition, leading to a deterioration in luminescence intensity.

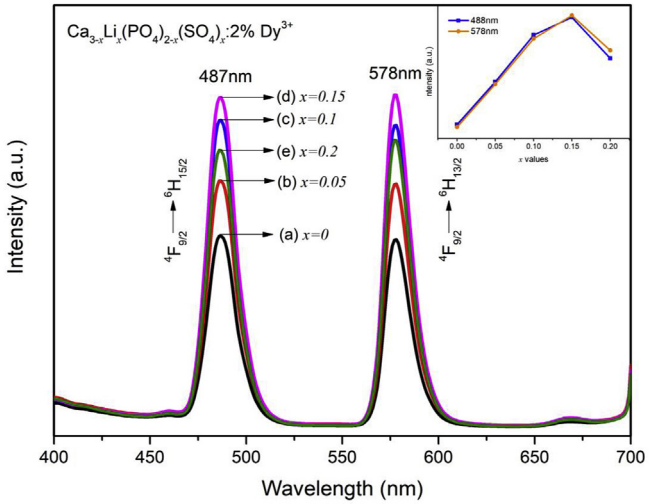

Fig. 4. Emission spectra (λ_{ex} = 352 nm) of $Ca_{3-x}Li_x(PO_4)_{2-x}(SO_4)_x$:2%$Dy^{3+}$ phosphors with different *x* values.

Inset of Fig. 4 depicted the dependence of the luminescence intensity of blue and yellow emission peaks of $Ca_{3-x}Li_x(PO_4)_{2-x}(SO_4)_x$:2%$Dy^{3+}$ phosphors on the substitution ration. The specific ration of I_{blue}/I_{yellow} can be obtained from Table 3. It can be seen that the calculated I_{blue}/I_{yellow} for $Ca_{3-x}Li_x(PO_4)_{2-x}(SO_4)_x$:2%$Dy^{3+}$ (x = 0.05, 0.1, 0.15 and 0.2) phosphors are 1.017, 1.012, 1.015, 0.993 and 0.965, respectively. The I_{blue}/I_{yellow} is usually used to determine the structural mismatch around Dy^{3+} ions, because the $^4F_{9/2} \rightarrow {}^6H_{15/2}$ belongs to magnetic dipole transition, which hardly affected by the surrounding of Dy^{3+}, and the $^4F_{9/2} \rightarrow {}^6H_{13/2}$ is under the control of electric dipole, which is sensitive to the surrounding

Table 3
I_{blue}/I_{yellow} of $Ca_{3-x}Li_x(PO_4)_{2-x}(SO_4)_x$:2%$Dy^{3+}$ phosphors with different *x* value.

x value	0	0.05	0.1	0.15	0.2
I_{blue}/I_{yellow}	1.017	1.012	1.015	0.993	0.965

of Dy^{3+} [42]. The hardly changed I_{blue}/I_{yellow} indicates that the local environment of Dy^{3+} maintains good stability after the incorporation of Li^{+} and S^{6+}, this confirms the conclusion from the XRD pattern that incorporation of Li^{+}/S^{6+} does not cause significant lattice distortion.

These phosphor samples were first optimized with $x = 0.15$, and then a series of experiments were carried out to check the influence of Dy^{3+} concentration on the luminescence intensity of the optimized phosphors sample. The XRD patterns of the $Ca_{2.85}Li_{0.15}(PO_4)_{1.85}(SO_4)_{0.15}$:$yDy^{3+}$ ($y = 0$, 0.01, 0.02, 0.03, 0.04 and 0.05) samples prepared with different Dy^{3+} concentrations are depicted in Fig. 5 There was no evident discrepancy between these XRD patterns of the as-prepared samples, and they matched well with the standard $Ca_3(PO_4)_2$ structure (PDF No. 09–0169). No evident impurity phases were observed, which indicated that the host structure was well retained at a low doping concentration of Dy^{3+}.

The excitation and emission spectra of the $Ca_{2.85}Li_{0.15}(PO_4)_{1.85}(SO_4)_{0.15}$:y Dy^{3+} ($y = 0$, 0.01, 0.02, 0.03, 0.04, and 0.05) phosphors containing various Dy^{3+} concentrations are shown in Fig. 6. A series of excitation peaks were observed from 300 to 450 nm. Specifically, the dominant excitation peaks were located at 352, 363 and 390 nm, which were derived from the $^6H_{15/2} \rightarrow {}^6P_{7/2}$, $^6H_{15/2} \rightarrow {}^6P_{7/2}$ and $^6H_{15/2} \rightarrow {}^4I_{13/2}$ transitions of Dy^{3+}, respectively. These results indicated that these phosphors could be excited efficiently by UV excitation. In the emission spectra of Fig. 6, two strong peaks are observed: blue emission (487 nm) and yellow emission (578 nm), which were ascribed to the $^4F_{9/2} \rightarrow {}^6H_{15/2}$ and $^4F_{9/2} \rightarrow {}^6H_{13/2}$ transitions of Dy^{3+}, respectively. Furthermore, it can also be seen that the luminescence intensity is dependent on the doping concentration of Dy^{3+}. Initially, increasing concentration favors intensity enhancement. However, a further increase of Dy^{3+} content degrades the emission intensity, so 3% is determined as the optimum concentration. Generally speaking, concentration quenching should be responsible for the declined intensity. The increase of Dy^{3+} concentration decreases the distance among them and will cause a higher probability of non-radiative (NR) transitions, which has no contribution to the emission intensity. As proposed by Blasse, the critical transfer distance (Rc) for activators in a specific host can be determined according to Eq. (1) [43]:

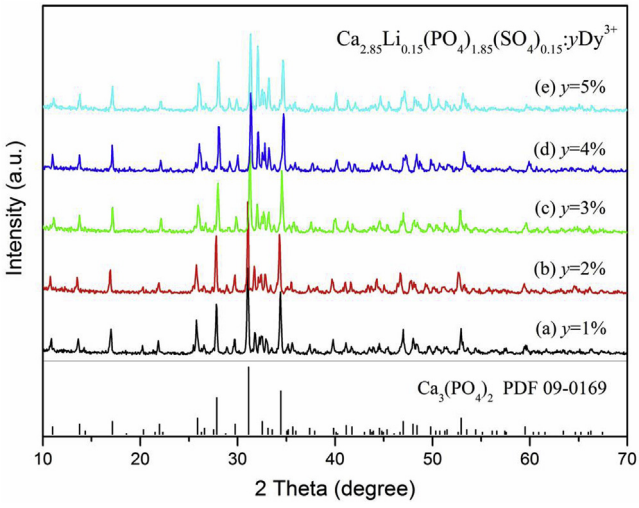

Fig. 5. XRD patterns of the $Ca_{2.85}Li_{0.15}(PO_4)_{1.85}(SO_4)_{0.15}$:$yDy^{3+}$ phosphors with different Dy^{3+} concentration.

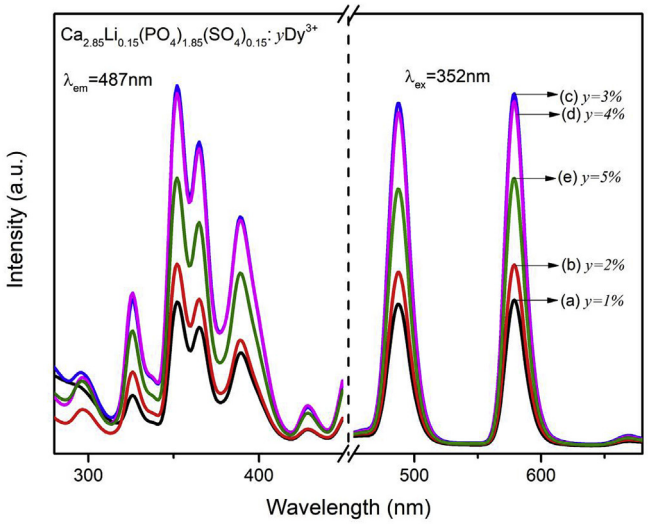

Fig. 6. Excitation and emission spectra of $Ca_{2.85}Li_{0.15}(PO_4)_{1.85}(SO_4)_{0.15}$:$Dy^{3+}$ phosphors with different Dy^{3+} concentration.

$$Rc = 2\left(\frac{3V}{4\pi x_c N}\right)^{1/3} \quad (1)$$

where V is the volume of the unit cell for $Ca_{2.85}Li_{0.15}(PO_4)_{1.85}(SO_4)_{0.15}$ (3520.06 Å^3); x_c is the critical concentration of Dy^{3+} (3%); and N is the number of formula units per unit cell (21). The Rc for $Ca_{2.85}Li_{0.15}(PO_4)_{1.85}(SO_4)_{0.15}$ was calculated to be 22.01 Å.

In fact, the mechanism of energy transfer should not be neglected for a thorough understanding of concentration quenching. The interactions for energy transfer can be summarized by three mechanisms: dipole-dipole, dipole-quadrupole, and quadrupole-quadrupole. Uitert et al. and Dexter et al. [44,45] proposed a quantitative description for the relationship between luminous intensity (I) and doping concentration (x), expressed according to Eq. (2):

$$I \Big/ x = k \Big/ \left[1 + \beta(x)^{Q/3}\right] \quad (2)$$

where k and β are constants for a certain matrix and Q represents the interaction mechanism. ($Q = 3$, 6, 8 or 10, representing the mechanisms that correspond to nearest-neighbor ions, dipole-dipole, dipole-quadrupole, and quadrupole-quadrupole, respectively) [46,47]. After an equivalent conversion, Eq. (2) can be represented according to Eq. (3):

$$\log(I/x) = C - \frac{Q}{3}\log(x) \quad (3)$$

where C is a constant. This indicates that the value of Q can be extracted by fitting the curves of $\log(I/x)$ vs. $\log(x)$. Fig. 7 depicts the relationship between $\log(I/x)$ and $\log(x)$. The slope of this linear fitting is −0.52, and the value of Q was obtained as 1.56, which is closest to 3 of 3, 6, 8, 10. It can be concluded that the interaction between nearest-neighbor ions is a dominant mechanism for concentration quenching.

Based on the optimized substitution ratio and doping concentration of Dy^{3+}, further investigation of the effect of Sm^{3+} co-doping on structure and luminescence was undertaken. Firstly, all of the XRD patterns of the $Ca_{2.85}Li_{0.15}(PO_4)_{1.85}(SO_4)_{0.15}$:3%$Dy^{3+}$, z$Sm^{3+}$ (z = 0, 0.5%, 1%, 2%, 3%) phosphors (Fig. 8) exhibited similar

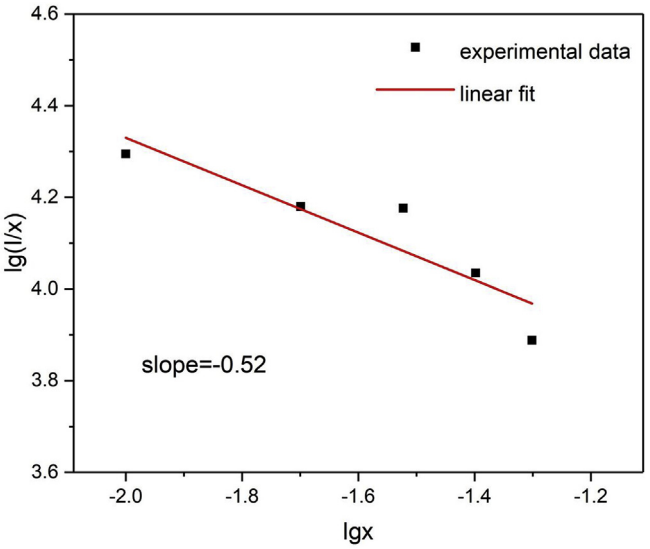

Fig. 7. The relationship between the concentration of Dy^{3+} ions log(x) versus log(I/x) of emission at 487 nm in $Ca_{2.85}Li_{0.15}(PO_4)_{1.85}(SO_4)_{0.15}$:$Dy^{3+}$ phosphors.

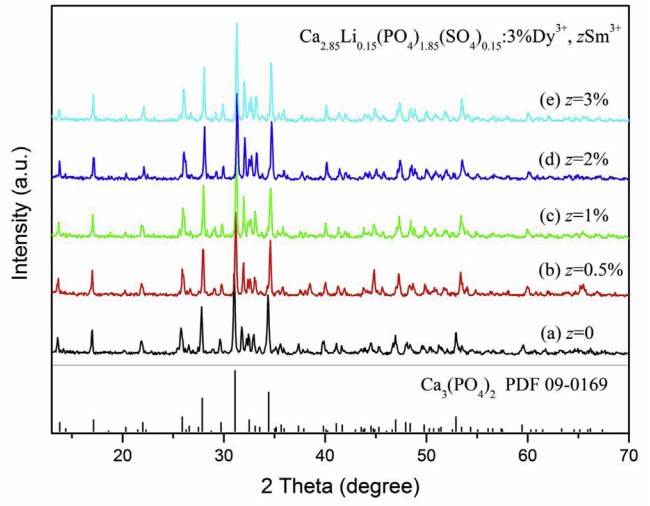

Fig. 8. XRD patterns of $Ca_{2.85}Li_{0.15}(PO_4)_{1.85}(SO_4)_{0.15}$:3%$Dy^{3+}$, $z$$Sm^{3+}$ phosphors with different Sm^{3+} co-doping concentrations.

diffraction peaks, which corresponded to the standard structure of $Ca_3(PO_4)_2$ (PDF No. 09−0169). This good consistency in XRD patterns indicated that Sm^{3+} (0.0958 nm) successfully entered the $Ca_3(PO)_4$ crystal lattice and substituted for Ca^{2+}(0.099 nm) sites, due to their similar ionic radii.

Subsequently, the investigation of Dy^{3+}/Sm^{3+} co-doping was carried out based on $Ca_{2.85}Li_{0.15}(PO_4)_{1.85}(SO_4)_{0.15}$ phosphors. Fig. 9 shows the emission spectra of $Ca_{2.85}Li_{0.15}(PO_4)_{1.85}(SO_4)_{0.15}$:3% Dy^{3+}, $z$$Sm^{3+}$ (z = 0.5%, 1%, 2%, 3%) at 352 nm excitation. In addition to the characteristic emission peaks of Dy^{3+} (blue and yellow), there appear two new orange-red emission peaks at 605 and 655 nm, respectively, which are originated from the $^4G_{5/2} \rightarrow {}^6H_{7/2}$ and $^4G_{5/2} \rightarrow {}^6H_{9/2}$ electron transitions of Sm^{3+}, respectively. This confirmed that Dy^{3+}/Sm^{3+} codoping is an effective method to produce red light emission and a superior warm white emission.

It is worth noting that the emission intensities of Dy^{3+} and Sm^{3+} showed opposite trends when the concentration of Sm^{3+} increased. As illustrated in the inset of Fig. 9, the luminescence intensity of

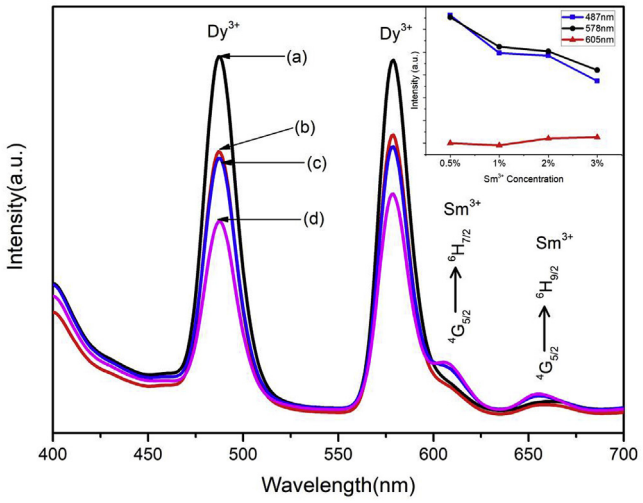

Fig. 9. Emission spectra of $Ca_{2.85}Li_{0.15}(PO_4)_{1.85}(SO_4)_{0.15}$:3%$Dy^{3+}$, $z$$Sm^{3+}$ with various Sm^{3+} concentration: (a) 0.5 mol%, (b) 1 mol%, (c) 2 mol%, (d) 3 mol%.

Dy^{3+} decreased while that of Sm^{3+} increased with increasing concentration of Sm^{3+}. This implied the existence of an energy transition between Dy^{3+} and Sm^{3+}.

Therefore, it was essential to investigate the specific transfer process. Energy transfer efficiency (η_{ET}) can be calculated according to Eq. (4) [48]:

$$\eta_{ET} = 1 - \frac{I_s}{I_{s0}} \tag{4}$$

where I_{s0} is the intrinsic luminescent intensity of Dy^{3+} and I_s is the luminescent intensity of Dy^{3+} in the presence of Sm^{3+}. Using Eq. (4), the energy transfers efficiencies from Dy^{3+} to Sm^{3+} were calculated to be 8%, 31%, 32.8% and 48.2% for the $Ca_{2.85}Li_{0.15}(PO_4)_{1.85}(SO_4)_{0.15}$:3%$Dy^{3+}$, $z$$Sm^{3+}$ (z = 0.5%, 1%, 2%, 3%) samples, respectively. The η_{ET} increased with increasing Sm^{3+} co-doping content, which revealed that the energy was transferred effectively from Dy^{3+} to Sm^{3+}.

To further confirm the energy transfer occurring between Dy^{3+} and Sm^{3+} ions, the luminescence lifetime (λ_{ex} = 352 nm and λ_{em} = 487 nm of Dy^{3+}) of $Ca_{2.85}Li_{0.15}(PO_4)_{1.85}(SO_4)_{0.15}$:3%$Dy^{3+}$, $z$$Sm^{3+}$ phosphors with different Sm^{3+} concentrations were measured and are shown in Fig. 10. The decay curves of $Ca_{2.85}Li_{0.15}(PO_4)_{1.85}(SO_4)_{0.15}$:3%$Dy^{3+}$, $z$$Sm^{3+}$ phosphors were well fitted by a double-exponential function given in the following equation [27]:

$$I(t) = I_0 + A_1 \exp\left(\frac{-t}{\tau_1}\right) + A_2 \exp\left(\frac{-t}{\tau_2}\right) \tag{5}$$

where I(t) corresponds to the luminescence intensity at time t, I_0 represents the initial intensity, A_1 and A_2 are the fitting parameters, and τ_1 and τ_2 are components of the decay time as a long lifetime and short lifetime, respectively. The double-exponential behavior indicates a heterogeneous distribution of Sm^{3+} ions in the $Ca_{2.85}Li_{0.15}(PO_4)_{1.85}(SO_4)_{0.15}$:3%$Dy^{3+}$, $z$$Sm^{3+}$ phosphors. The average lifetime was evaluated by the following formula [35]:

$$\tau_{av} = \frac{(A_1\tau_1^2 + A_2\tau_2^2)}{(A_1\tau_1 + A_2\tau_2)} \tag{6}$$

From Eq. (6) and Fig. 10, the effective lifetime values for $Ca_{2.85}Li_{0.15}(PO_4)_{1.85}(SO_4)_{0.15}$:3%$Dy^{3+}$, $z$$Sm^{3+}$ phosphors with z = 0,

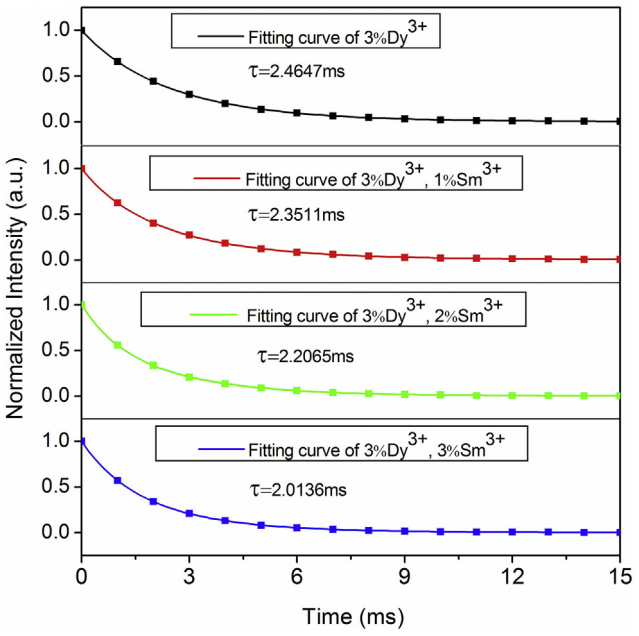

Fig. 10. The decay curves ($\lambda_{em} = 487$ nm) of $Ca_{2\cdot85}Li_{0\cdot15}(PO_4)_{1\cdot85}(SO_4)_{0.15}$:3%$Dy^{3+}$, z$Sm^{3+}$ ($z = 0$, 1%, 2% and 3%) phosphors.

1%, 2%, and 3% were calculated as 2.4647 ms, 2.3511 ms, 2.2065 ms and 2.0136 ms, respectively. The luminescence lifetime of Dy^{3+} was shortened by an increase in Sm^{3+} ion concentration; therefore, there was a significant energy transfer from Dy^{3+} to Sm^{3+} ions in $Ca_{2\cdot85}Li_{0\cdot15}(PO_4)_{1\cdot85}(SO_4)_{0.15}$.

For a further illustration for the energy transfer from Dy^{3+} to Sm^{3+} (R_{Dy-Sm}). Herein, we calculated the critical distance between Dy^{3+} and Sm^{3+}, which can be described as the following equation (7).

$$R_{Dy-Sm} = 2\left(\frac{3V}{4\pi x_c N}\right)^{1/3} \quad (7)$$

where V equals to 3526.77 $Å^3$, and N equals to 21 as mentioned earlier in Eq. (1). Also, x_c represents the sum of the concentrations of Dy^{3+} and Sm^{3+} activator ions. Thus, the calculated R_{Dy-Sm} is 17.48 Å for 3% Dy^{3+} and 3%Sm^{3+}. which is much larger than the typical critical distance (5 Å) for exchange interaction. The results indicate that the multipolar interaction occurs in the energy-transfer process. As the concentration of Sm^{3+} increases, the distance between Dy^{3+} and Sm^{3+} becomes shorter. Besides, the energy difference between $^4F_{9/2}$ and $^6H_{I/2}$ ($I = 13$, 15) of Dy^{3+} is approximately in accordance with that of $^4G_{5/2}$ and $^6H_{J/2}$ ($J = 7$, 9) of Sm^{3+}. These factors accelerate the energy transfer to occur between Dy^{3+} and Sm^{3+} activators [49], causing the changes in emission intensity and luminescence lifetime.

A schematic of the specific energy transition process is provided in Fig. 11. Under suitable excitation, the ^6H electrons of the Dy^{3+} ions are excited to a high energy level, then return to the lower energy level $^4F_{9/2}$ through a non-radiative (NR) transition. Subsequently, electrons tend to fall into lower energy levels and emit photons in the process, which are radiative transitions. With the incorporation of Sm^{3+}, some of the electrons excited from Dy^{3+} have a higher possibility of transfer to the $^4G_{5/2}$ level of Sm^{3+} rather than the lower energy level of Dy^{3+} because of the closeness of this energy level, and these electrons contribute to the Sm^{3+} emission. This electron behavior accounts for the discrepancy in the luminescence intensity trend for Dy^{3+} and Sm^{3+}. The external quantum

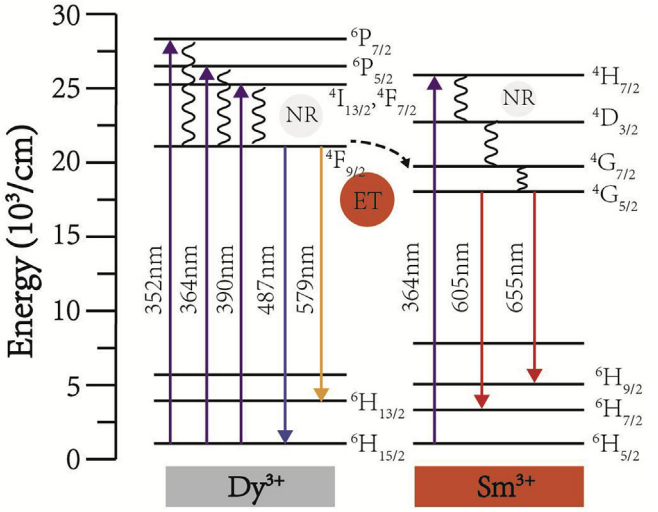

Fig. 11. The energy level diagrams of Dy^{3+} and Sm^{3+} with possible energy transfer processes.

efficiency of $Ca_{2\cdot85}Li_{0\cdot15}(PO_4)_{1\cdot85}(SO_4)_{0.15}$:3%$Dy^{3+}$, 2%$Sm^{3+}$ samples was 21.7%, which is a good result for prospective applications.

Thermal stability is one of the most critical parameters for phosphors in their practical LED application because it has a significant impact on *CRI* and the light output. Fig. 12 presents the luminescence thermal quenching results of $Ca_{2\cdot85}Li_{0\cdot15}(PO_4)_{1\cdot85}(SO_4)_{0.15}$:3%$Dy^{3+}$, 2%$Sm^{3+}$ phosphor over the temperature range from 25 °C to 150 °C. With the increase in temperature, the emission intensity decreases gradually. As a result, the emission intensity at 150 °C drops to 71.6% of the corresponding values at 25 °C for $Ca_{2\cdot85}Li_{0\cdot15}(PO_4)_{1\cdot85}(SO_4)_{0.15}$:3% Dy^{3+}, 2%Sm^{3+}. The emission intensity decreases due to non-radiative loss of energy when the temperature increases because vibrational states reach the intersection between ground state and charge transfer band at high temperature. As the emission intensity of the phosphor is still satisfactory at high temperature, it can be concluded that the $Ca_{2\cdot85}Li_{0\cdot15}(PO_4)_{1\cdot85}(SO_4)_{0.15}$:3%$Dy^{3+}$, 2%$Sm^{3+}$ phosphor exhibit good thermal stability, and serve as a potential phosphor candidate for solid-state lighting.

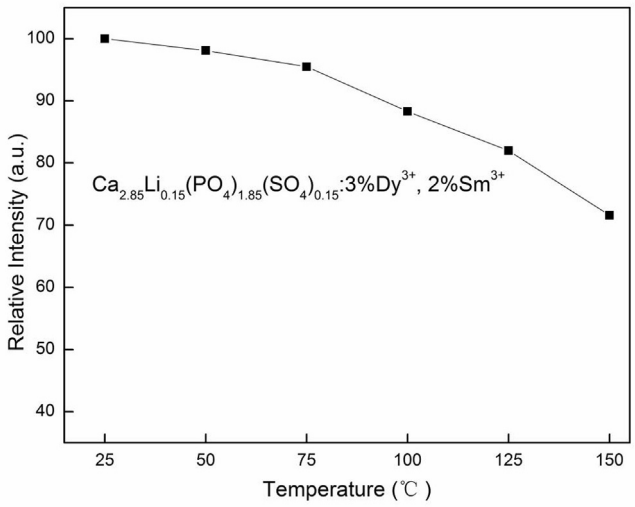

Fig. 12. The luminescence thermal quenching of $Ca_{2\cdot85}Li_{0\cdot15}(PO_4)_{1\cdot85}(SO_4)_{0.15}$: 3%$Dy^{3+}$, 2%$Sm^{3+}$ phosphor.

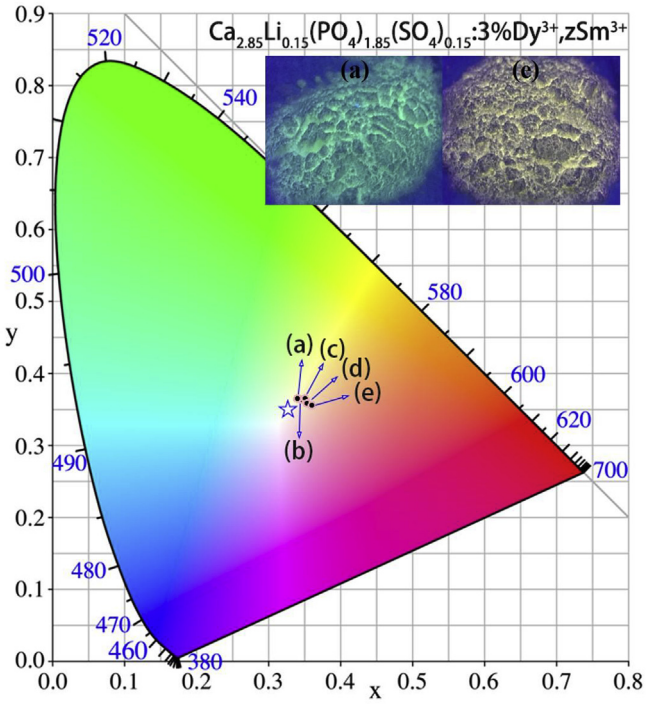

Fig. 13. CIE coordinates of $Ca_{2.85}Li_{0.15}(PO_4)_{1.85}(SO_4)_{0.15}$:3%$Dy^{3+}$, z$Sm^{3+}$ with different Sm^{3+} concentrations: (a) z = 0, (b) z = 0.5%, (c) z = 1%, (d) z = 2%, (e) z = 3%.

The CIE chromaticity coordinates of the $Ca_{2.85}Li_{0.15}(PO_4)_{1.85}(SO_4)_{0.15}$:3%$Dy^{3+}$, z$Sm^{3+}$ samples are shown in Fig. 13. The standard white light point is marked with a white pentagram, it can be seen that these samples are all located in the white region. The specific chromaticity coordinate data are provided in Table 4, confirming that all the samples showed good white emission performance. And, more importantly, with increasing Sm^{3+}concentration the light was red-shifted and showed superior warm white emission performance. Since red light emission was provided through Sm^{3+} co-doping, these samples exhibited a better warm white emission.

The *CCT* is considered as an important indicator for evaluating lighting quality. According to the proposed theory [50], the *CCT* values of these phosphors were calculated via Eq. (8):

$$CCT = -449n^3 + 3525n^2 - 6823n + 5520.33 \quad (8)$$

where $n = (x - x_e)/(y - y_e)$, x_e and y_e equal 0.3320 and 0.1858, respectively. The resulting calculated *CCT* values are shown in Table 4. It can be seen that the *CCT* generally decreased with increasing Sm^{3+} doping, confirming that these samples exhibited superior warm white performance when red emission was stronger. $Ca_{2.85}Li_{0.15}(PO_4)_{1.85}(SO_4)_{0.15}$:3% Dy^{3+}, 3%Sm^{3+} ($x = 0.3614$, $y = 0.3556$) in particular showed good warm white light performance with a *CCT* of 4281 K (Warm White). The result shows that it is feasible and efficient to adjust the performance of the phosphor by co-doping with rare-earth ions, and the optimized co-doped $Ca_{2.85}Li_{0.15}(PO_4)_{1.85}(SO_4)_{0.15}$:3% Dy^{3+}, 3%Sm^{3+} phosphor has the potential to be applied as a new single-component phosphor.

Table 4
The CIE chromaticity coordinates (x, y) of $Ca_{2.85}Li_{0.15}(PO_4)_{1.85}(SO_4)_{0.15}$:3%$Dy^{3+}$, z$Sm^{3+}$.

Spot	Sample	CIE X	CIE Y	*CCT*(*K*)	Light color
(a)	3%Dy^{3+}	0.3399	0.3651	5226	Cool white light
(b)	3%Dy^{3+}, 0.5%Sm^{3+}	0.3446	0.3637	5054	Cool white light
(c)	3%Dy^{3+}, 1% Sm^{3+}	0.3513	0.3652	4827	Neutral white light
(d)	3%Dy^{3+}, 2% Sm^{3+}	0.3528	0.3588	4650	Neutral white light
(e)	3%Dy^{3+}, 3% Sm^{3+}	0.3604	0.3566	4281	Warm white light

4. Conclusion

In summary, a series of $Ca_{3-x}Li_x(PO_4)_{2-x}(SO_4)_x$:$Dy^{3+}$, Sm^{3+} samples were synthesized by a sol-gel method. The structure of all samples maintained good consistency in structure with $Ca_3(PO_4)_2$, unaffected by partial substitution and rare earth ion doping. Under an appropriate excitation of 352 nm, the $Ca_{3-x}Li_x(PO_4)_{2-x}(SO_4)_x$:$Dy^{3+}$ phosphors exhibited two emission peaks at 487 nm (blue) and 578 nm (yellow), which could achieve white light emission. The partial substitution of Ca^{2+}/P^{5+} with Li^+/S^{6+} ion pairs significantly enhanced the luminescence intensity of $Ca_{3-x}Li_x(PO_4)_{2-x}(SO_4)_x$:$Dy^{3+}$ samples and the optimum value of *x* was determined as 0.15. Furthermore, with the incorporation of Sm^{3+}, the phosphors showed improved warm emission and lower *CCT* value (4281 K) due to the presence of red emissions. Its external quantum efficiency was measured as 21.7%. This study demonstrates that the optimized phosphate phosphors obtained by combining partial substitution and Dy^{3+}/Sm^{3+} co-doping have the potential to be used in warm *w*-LEDs.

Declaration of competing interest

The authors declare that they have no known competing financial interests or personal relationships that could have appeared to influence the work reported in this paper.

Acknowledgements

This work was financially supported by Sichuan Science and Technology Program (No. 2017SZ0185, 2018SZDZX0022).

Appendix A. Supplementary data

Supplementary data to this article can be found online at https://doi.org/10.1016/j.jallcom.2019.152761.

References

[1] E.F. Schubert, J.K. Kim, Solid-state light sources getting smart, Science 308 (2005) 1274–1278.
[2] T. Hashimoto, F. Wu, J.S. Speck, S. Nakamura, A GaN bulk crystal with improved structural quality grown by the ammonothermal method, Nat. Mater. 6 (2007) 568–571.
[3] P.F. Smet, A.B. Parmentier, D. Poelman, Selecting conversion phosphors for white light-emitting diodes, J. Electrochem. Soc. 158 (2011) R37–R54.
[4] Z. Luo, G. Qi, K. Chen, M. Zou, L. Yuwen, X. Zhang, W. Huang, L. Wang, Microwave-assisted preparation of white fluorescent graphene quantum dots as a novel phosphor for enhanced white-light-emitting diodes, Adv. Funct. Mater. 26 (2016) 2739–2744.
[5] Z. Xia, A. Meijerink, Ce^{3+}-doped garnet phosphors: composition modification, luminescence properties and applications, Chem. Soc. Rev. 46 (2017) 275–299.
[6] H.-R. Chen, C. Cai, Z.-W. Zhang, L. Zhang, H.-P. Lu, X. Xu, H.V. Bui, K.-H. Qiu, L.-J. Yin, Enhancing the luminescent efficiency of $Y_3Al_5O_{12}$:Ce^{3+} by coating graphitic carbon nitride: toward white light-emitting diodes, J. Alloy. Comp. 801 (2019) 10–18.
[7] A.A. Setlur, W.J. Heward, Y. Gao, A.M. Srivastava, R.G. Chandran, M.V. Shankar, Crystal chemistry and luminescence of Ce^{3+}-doped $Lu_2CaMg_2(Si,Ge)_3O_{12}$ and its use in LED based lighting, Chem. Mater. 18 (2006) 3314–3322.
[8] W. Zhang, Y. Wang, Y. Gao, J. Long, J. Li, Sol-gel assisted synthesis and photoluminescence property of $Sr_2Si_5N_8$:Eu^{2+}, Dy^{3+} red phosphor for white light emitting diodes, J. Alloy. Comp. 667 (2016) 341–345.
[9] J. Xie, F. Zhang, G. Li, W. Zhang, Effect of crystal structures on energy transfer behavior from Bi^{3+} to Eu^{3+} in alkaline earth metal stannates, Ceram. Int. 43 (2017) 12026–12034.

[10] S.-H. Zhang, H.-R. Chen, C. Cai, Z.-W. Zhang, Y.-J. Zhao, L. Zhang, X. Wang, L.-B. Zhang, X. Xu, H.V. Bui, L.-J. Yin, Achieving an efficient $La_3Si_8N_{11}O_4$: Eu^{2+} phosphor via chemical reduction of nano-scale carbon film: toward white light-emitting diodes, J. Alloy. Comp. 799 (2019) 360–367.

[11] Z. Leng, R. Li, L. Li, D. Xue, D. Zhang, G. Li, X. Chen, Y. Zhang, Preferential neighboring substitution-triggered full visible spectrum emission in single-phased $Ca_{10.5-x}Mg_x(PO_4)_7$:Eu^{2+} phosphors for high color-rendering white LEDs, ACS Appl. Mater. Interfaces 10 (2018) 33322–33334.

[12] S. Som, P. Mitra, V. Kumar, V. Kumar, J.J. Terblans, H.C. Swart, S.K. Sharma, The energy transfer phenomena and colour tenability in Y_2O_2S:Eu^{3+}/Dy^{3+} microfibers for white emission in solid state lighting applications, Dalton Trans. 43 (2014) 9860–9871.

[13] S. Kaur, A.S. Rao, M. Jayasimhadri, B. Sivaiah, D. Haranath, Synthesis optimization, photoluminescence and thermoluminescence studies of Eu^{3+} doped calcium aluminozincate phosphor, J. Alloy. Comp. 802 (2019) 129–138.

[14] W. Shan, L. Wu, N. Tao, Y. Chen, D. Guo, Optimization method for green $SrAl_2O_4$:Eu^{2+}, Dy^{3+} phosphors synthesized via co-precipitation route assisted by microwave irradiation using orthogonal experimental design, Ceram. Int. 10 (2015) 15034–15040.

[15] Y. Wang, W. Zhang, X. Chen, H. Du, J. Li, K. Qiu, Influence of Al^{3+}/P^{5+} ions substitution on the structure and luminescence properties of Sr_2SiO_4:Eu^{2+} phosphors for white light emitting diodes, Ceram. Int. 43 (2017) 2824–2828.

[16] S.A. Khan, N.Z. Khan, Z. Hao, W.W. Ji, H. Abadikhah, L. Hao, X. Xu, S. Agathopoulos, Influence of substitution of Al-O for Si-N on improvement of photoluminescence properties and thermal stability of $Ba_2Si_5N_8$:Eu^{2+} red emitting phosphors, J. Alloy. Comp. 730 (2018) 249–254.

[17] W. Ji, Z. Xia, K. Liu, S.A. Khan, L. Hao, X. Xu, L. Yin, M.S. Molokeev, S. Agathopoulos, W. Yang, X. Ma, K. Sun, I. da Silva, The crystal structure and luminescence properties of a novel green-yellow emitting $Ca_{1.5}Mg_{0.5}Si_{1-x}Li_xO_{4-\delta}$:$Ce^{3+}$ phosphor with high quantum efficiency and thermal stability, Dalton Trans. 47 (2018) 9834–9844.

[18] A.K. Sharma, K.H. Son, B.Y. Han, K.-S. Sohn, Simultaneous optimization of luminance and color chromaticity of phosphors using a nondominated sorting genetic algorithm, Adv. Funct. Mater. 20 (2010) 1750–1755.

[19] A. Balakrishna, H.C. Swart, R. Ramaraghavulu, A.K. Bedyal, R.E. Kroon, O.M. Ntwaeaborwa, Structural evolution induced by substitution of designately $(MoO_4)^{2-}$ by different groups (BO_3^{3-}, PO_4^{3-}, SO_4^{2-}) in $CaMoO_4$:Sm^{3+} phosphors-a study on color tunable luminescent properties, J. Alloy. Comp. 727 (2017) 224–237.

[20] Y. Liu, B. Lei, C. Shi, Luminescent properties of a white afterglow phosphor $CdSiO_3$:Dy^{3+}, Chem. Mater. 17 (2005) 2108–2113.

[21] B.V. Ratnam, M. Jayasimhadri, K. Jang, H.S. Lee, S.S. Yi, J.H. Jeong, White light emission from $NaCaPO_4$:Dy^{3+} phosphor for ultraviolet-based white light-emitting diodes, J. Am. Ceram. Soc. 93 (2010) 3857–3861.

[22] J. Long, F. Chu, Y. Wang, C. Zhao, W. Dong, X. Yuan, C. Ma, Z. Wen, R. Ma, M. Du, Y. Cao, $M_8MgSc(PO_4)_7$:xDy^{3+} (M = Ca/Sr) single-phase full-color phosphor with high thermal emission stability, Inorg. Chem. 56 (2017) 10381–10386.

[23] H. Yu, L. Su, X. Qian, D. Jiang, Q. Wu, F. Tang, J. Wang, J. Xu, Influence of Gd^{3+} on the optical properties of Dy^{3+}-activated CaF_2 single crystal for white LED application, J. Electron. Mater. 48 (2019) 2910–2915.

[24] A. Balakrishnaa, O.M. Ntwaeaborwa, Study of luminescent behavior and crystal defects of different $MNa[PO_4]$-Dy^{3+} phosphors (M = Mg, Ca, Sr and Ba), Sens. Actuators B Chem. 242 (2017) 305–317.

[25] A. Lecointre, A. Bessière, A.J.J. Bos, P. Dorenbos, B. Viana, S. Jacquart, Designing a red persistent luminescence phosphor: the example of YPO_4:Pr^{3+},Ln^{3+} (Ln = Nd, Er, Ho, Dy), J. Phys. Chem. C 115 (2011) 4217–4227.

[26] S.A. Khan, H. Zhong, W. Ji, L.-Y. Hao, H. Abadikhah, X. Xu, N.Z. Khan, S. Agathopoulos, Single-phase white light-emitting $Ca_xBa_{(9-x)}Lu_2Si_6O_{24}$:$Eu^{2+}$/$Mn^{2+}$ phosphors, ACS Omega 2 (2017) 6270–6277.

[27] Y. Gan, W. Liu, W. Zhang, W. Li, Y. Huang, K. Qiu, Effects of Gd^{3+} codoping on the enhancement of the luminescent properties of a $NaBi(MoO_4)_2$:Eu^{3+} red-emitting phosphors, J. Alloy. Comp. 784 (2019) 1003–1010.

[28] Y. Chen, J. Wang, C. Liu, X. Kuang, Q. Su, A host sensitized reddish-orange Gd_2MoO_6:Sm^{3+} phosphor for light emitting diodes, Appl. Phys. Lett. 98 (2011) 081917.

[29] S. Kaur, A.S. Rao, M. Jayasimhadri, Spectroscopic and photoluminescence characteristics of Sm^{3+} doped calcium aluminozincate phosphor for applications in w-LED, Ceram. Int. 43 (2017) 7401–7407.

[30] S. Gaikwad, Y. More, R.R. Patil, M.S. Kulkarni, B.C. Bhatt, S.V. Mohari, Optically stimulated luminescence in doped $K_3Na(SO_4)_2$ phosphors, Radiat. Meas. 93 (2016) 20–27.

[31] K. Li, Y. Zhang, X. Li, M. Shang, H. Lian, J. Lin, Tunable blue-green emission and energy transfer properties in β-$Ca_3(PO_4)_2$:Eu^{2+}, Tb^{3+} phosphors with high quantum efficiencies for UV-LEDs, Dalton Trans. 44 (2015) 4683–4692.

[32] F. Zhang, J. Xie, G. Li, W. Zhang, Y. Wang, Y. Huang, Y. Tao, Cation composition sensitive visible quantum cutting behavior of high efficiency green phosphors $Ca_9Ln(PO_4)_7$:Tb^{3+} (Ln = Y, La, Gd), J. Mater. Chem. C 5 (2017) 872–881.

[33] Z. Hu, Y. Guo, J. Zhang, Y. Zhang, Tunable luminescence properties and energy transfer of single-phase $Ca_4(PO_4)_2O$: Dy^{3+}, Eu^{2+} multi-color phosphors for warm white light, J. Mater. Sci. 53 (2018) 6414–6423.

[34] X. Zhang, L. Zhou, M. Gong, High-brightness Eu^{3+}-doped $Ca_3(PO_4)_2$ red phosphor for NUV light-emitting diodes application, Opt. Mater. 35 (2013) 993–997.

[35] J. Fan, W. Zhang, S. Dai, G. Yan, M. Deng, K. Qiu, Effect of charge compensators A^+ (A = Li, Na and K) on luminescence enhancement of $Ca_3Sr_3(PO_4)_4$:Sm^{3+} orange-red phosphors, Ceram. Int. 44 (2018) 20028–20033.

[36] Y. Li, H. Yu, D. Deng, Y. Hua, S. Zhao, G. Jia, H. Wang, L. Huang, Y. Li, C. Li, S. Xu, Color point tuning by partial Ba^{2+} substitution of Ca^{2+} in $(Ca_{1-x}Ba_x)_3(PO_4)_2$: Eu^{2+} phosphor for white light emitting diodes, J. Solid State Chem. 199 (2013) 248–252.

[37] D. Kim, S.-C. Kim, J.-S. Bae, S. Kim, S.-J. Kim, J.-C. Park, Eu^{2+}-activated alkaline-earth halophosphates, $M_5(PO_4)_3X$:Eu^{2+} (M = Ca, Sr, Ba; X = F, Cl, Br) for NUV-LEDs: site-selective crystal field effect, Inorg. Chem. 55 (2016) 8359–8370.

[38] K. Kumar Gupta, R.M. Kadam, N.S. Dhoble, S.P. Lochab, V. Singh, S.J. Dhoble, Photoluminescence, thermoluminescence and evaluation of some parameters of Dy^{3+} activated $Sr_5(PO_4)_3F$ phosphor synthesized by sol-gel method, J. Alloy. Comp. 688 (2016) 982–993.

[39] H. Ji, Z. Huang, Z. Xia, M.S. Molokeev, V.V. Atuchin, S. Huang, Cation substitution dependent bimodal photoluminescence in whitlockite structural $Ca_{3-x}Sr_x(PO_4)_2$:Eu^{2+} ($0 \leq x \leq 2$) solid solution phosphors, Inorg. Chem. 53 (2014) 11119–11124.

[40] G. Chen, F. Wang, J. Yu, H. Zhang, X. Zhang, Improved red emission by codoping Li^+ in $ZnWO_4$:Eu^{3+} phosphors, J. Mol. Struct. 1128 (2017) 1–4.

[41] A.K. Parchur, A.I. Prasad, S.B. Rai, R.S. Ningthoujam, Improvement of blue, white and NIR emissions in YPO_4:Dy^{3+} nanoparticles on co-doping of Li^+ ions, Dalton Trans. 41 (2012) 13810–13814.

[42] Q. Su, Z. Pei, L. Chi, H. Zhang, Z. Zhang, F. Zou, The yellow-to-blue intensity ratio (*Y*/*B*) of Dy^{3+} emission, J. Alloy. Comp. 192 (1993) 25–27.

[43] G. Blasse, Energy transfer in oxidic phosphors, Phys. Lett. A 28 (1968) 444–445.

[44] D. Dexter, J.H. Schulman, Theory of concentration quenching in inorganic phosphors, J. Chem. Phys. 22 (1954) 1063–1070.

[45] V. Uitert, Characterization of energy transfer interactions between rare earth ions, J. Electrochem. Soc. 114 (1967) 1048–1053.

[46] T. Wang, Y. Hu, L. Chen, X. Wang, M. He, An intense red-emitting phosphor $Sr_3Lu(PO_4)_3$:Eu^{3+} for near ultraviolet light emitting diodes application, Ceram. Int. 42 (2016) 3659–3665.

[47] B. Devakumar, P. Halappa, C. Shivakumara, Dy^{3+}/Eu^{3+} co-doped $CsGd(MoO_4)_2$ phosphor with tunable photoluminescence properties for near-UV WLEDs applications, Dyes Pigments 137 (2017) 244–255.

[48] B. Li, X. Huang, H. Guo, Y. Zeng, Energy transfer and tunable photoluminescence of $LaBWO_6$:Tb^{3+},Eu^{3+} phosphors for near-UV white LEDs, Dyes Pigments 150 (2018) 67–72.

[49] D. Balaji, K. Kavirasu, A. Durairajan, S.M. Babu, Photoluminescence properties of novel Sm^{3+} and Dy^{3+} co-activated $CsGd(WO_4)_2$ phosphors, J. Alloy. Comp. 637 (2015) 350–360.

[50] C.S. Mccamy, Correlated color temperature as an explicit function of chromaticity coordinates, Color Res. Appl. 17 (1992) 142–144.